

MAGNETIC TOPOLOGY IN 1998 NOVEMBER 5 TWO-RIBBON FLARE AS INFERRED FROM GROUND-BASED OBSERVATIONS AND LINEAR FORCE-FREE FIELD MODELING

V. B. YURCHYSHYN,^{1,2} H. WANG,¹ J. QIU,¹ P. R. GOODE,¹ AND V. I. ABRAMENKO²

Received 1999 November 28; accepted 2000 March 28

ABSTRACT

We analyzed the three-dimensional structure of the linear force-free magnetic field. A longitudinal magnetogram of Active Region NOAA 8375 has been used as the photospheric boundary condition. The 1998 November 5 2B/M8.4 two-ribbon flare can be explained in the framework of quadrupolar reconnection theory: the interaction of two closed magnetic loops that have a small spatial angle. The energy derived from soft X-ray telescope (SXT)/*Yohkoh* data ($3\text{--}6 \times 10^{30}$ ergs) is 1 order of magnitude higher than the lower limit of flare energy predicted by Melrose's model. The latter estimation was made using the linear force-free extrapolation. It was suggested that, taking into account the nonlinear character of the observed magnetic field, we can increase the lower limit of the magnetic energy stored in the studied magnetic configuration. The revealed magnetic configuration allows us to understand the observed location and evolution of the flare ribbons and the additional energy released during the gradual phase of the flare, as well. Besides, reconnection of closed magnetic loops can logically explain the connection between a two-ribbon flare and a giant X-ray postflare arch, which usually is observed after the flare onset. We emphasize that unlike the Kopp and Pneuman configuration, the model discussed here does not necessarily require destabilization and opening of the magnetic field.

Subject headings: Sun: flares — Sun: magnetic fields

1. INTRODUCTION

It is generally accepted that a two-ribbon flare (TRF) is due to a reconnection process that happens in a previously open magnetic field (Sturrock 1968; Hirayama 1974; Kopp & Pneuman 1976). It suggests that rising prominences and/or fast expanding coronal loops are triggers of the TRF. After magnetic field destabilization and eruption, the stretched magnetic field lines become open and reconnect. This process is accompanied by type III and IV radio bursts.

On the other hand, it has also been shown that there is no direct link between filament eruption and TRFs (Forbes 1992). Out of 16 studied two-ribbon flares with preexisting dark filament, in 10 cases filaments erupted, and 5 filaments remained undisturbed (Hirayama 1974). In an earlier study by Smith & Ramsey (1964), about half of the major flares were found to be associated with active region filaments and preceded by their sudden eruption.

Ogir (1967) revealed that some TRFs are not followed by type IV radio bursts and their appearance in radio waves is rather weak. Moreover, those TRFs without radio emission are different from ones that gave a radio signal. The latter type originated as one narrow chromospheric ribbon, which some minutes later split up into two narrow, parallel ribbons showing a large separation, while flare ribbons in TRFs without radio emission were separated at the very beginning of the flaring process.

A simple study of $H\alpha$ images of major solar flares shows that we deal with two kinds of TRFs. The first one consists of flares with nearly parallel and straight ribbons located on opposite sides of the neutral line. Also, footpoints of the postflare loop (PFL) system cover the entire flare ribbons (Fig. 2 in Schmieder 1992; Fig. 8 in Rust & Bar 1973), and the PFL system itself is in a potential state (Roy 1972) or

has a more complicated structure (Rust & Bar 1973). One prominent feature of this kind of flare is the ribbon separation. Direct measurements show that the speed of the apparent expansion falls between 10 and 60 km s⁻¹ (Ogir 1967; Hirayama 1974; Loughhead, Chen, & Wang 1984; Gu et al. 1992; Korobova & Sajdalieva 1993). Such TRFs might be well described by the Kopp & Pneuman configuration (Fig. 1 in Kopp & Pneuman 1976).

Another kind of TRF may be described as follows. The flare ribbons are curved and are not located opposite each other. Footpoints of the postflare loop system cover only part of the flare ribbons (Fig. 5 in Heinzel, Schmieder, & Mein 1992; Figs. 2 and 3 in Tang 1985; Figs. 2 and 3, present paper). The flare ribbons do not show any significant separation in the course of the flare, and at the very beginning they are situated far from the active region neutral line (de la Beaujardiere et al. 1995). One of the flare ribbons may reach the leading sunspot and cover it partially (Fig. 2 in Lin, Zhang, & Zhang 1993; Fig. 1 in Gu et al. 1992).

Any flare model must explain not only how and where magnetic energy is released, but also a location, a shape, and a topological link between all flare ribbons and remote brightenings seen in the course of a two-ribbon flare.

The Hard X-ray Imaging Spectrometer aboard the *SMM* mission discovered extensive postflare coronal arches (Švestka et al. 1982). The arches appeared to be connected to the occurrence of two-ribbon flares. The loops reached altitudes in excess of 150,000 km in the solar corona and could be seen in *X-ray* for 10 hr or more (Švestka 1984). These arches either were rising in the corona or were stationary. Rising arches are related to coronal mass ejections (CMEs), while stationary ones are not (Švestka et al. 1995; Fárník et al. 1996). To explain the observed phenomena, Kopp & Poletto (1990) introduced a complex magnetic configuration that consists of two different systems of field lines that open and reconnect, producing a postflare loop system and a giant coronal arch. Šimberová, Karlický, & Švestka

¹ Big Bear Solar Observatory, Big Bear City, CA 92314.

² Crimean Astrophysical Observatory, 98409, Nauchny, Crimea, Ukraine.

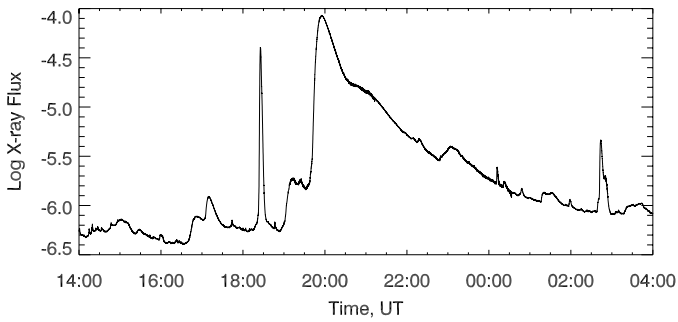


FIG. 1.—GOES X-ray time profile of 1998 November 5 flare

(1993) also showed that the 1973 August 13/14 soft X-ray *Skylab* postflare arch was formed by interactions of large-scale loops present above the flaring active region. This result does not seem to support the Kopp & Pneuman (1976) model, which invokes the reconnection of the open magnetic field lines. To the contrary, the coexistence of a giant X-ray postflare arch and a postflare loop system in the course of a two-ribbon flare can be a sign of a single reconnection event in a simple magnetic system of closed coronal loops.

For the famous, well-studied 1981 May 16 two-ribbon flare, Vrřnak et al. (1987) established that the site of energy

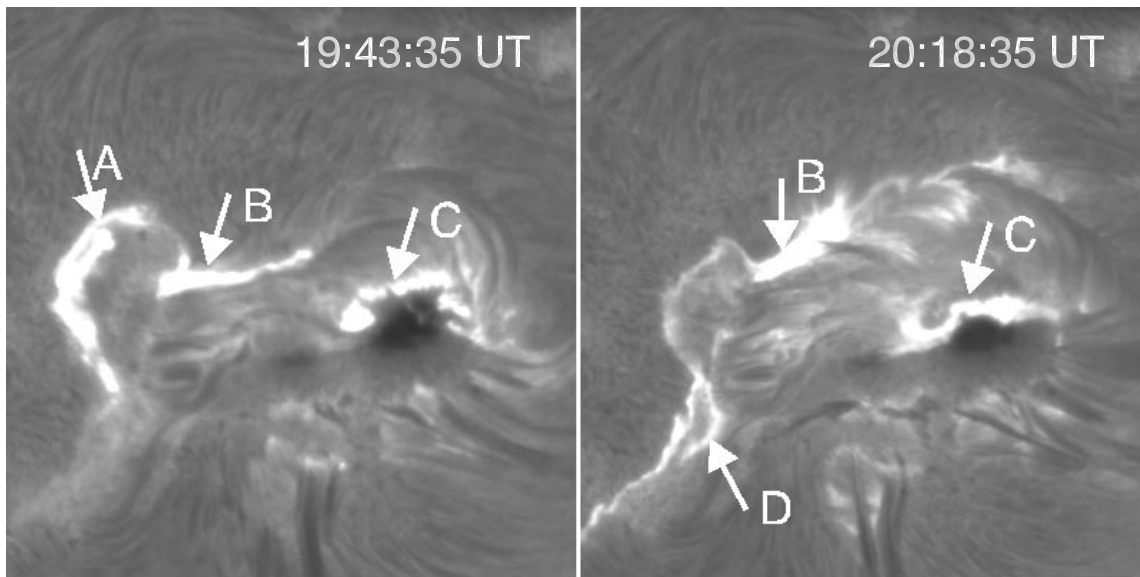


FIG. 2.— $H\alpha$ images of the two-ribbon flare obtained on 1998 November 5. The images are from 65 cm telescope; the field of view is $200'' \times 200''$.

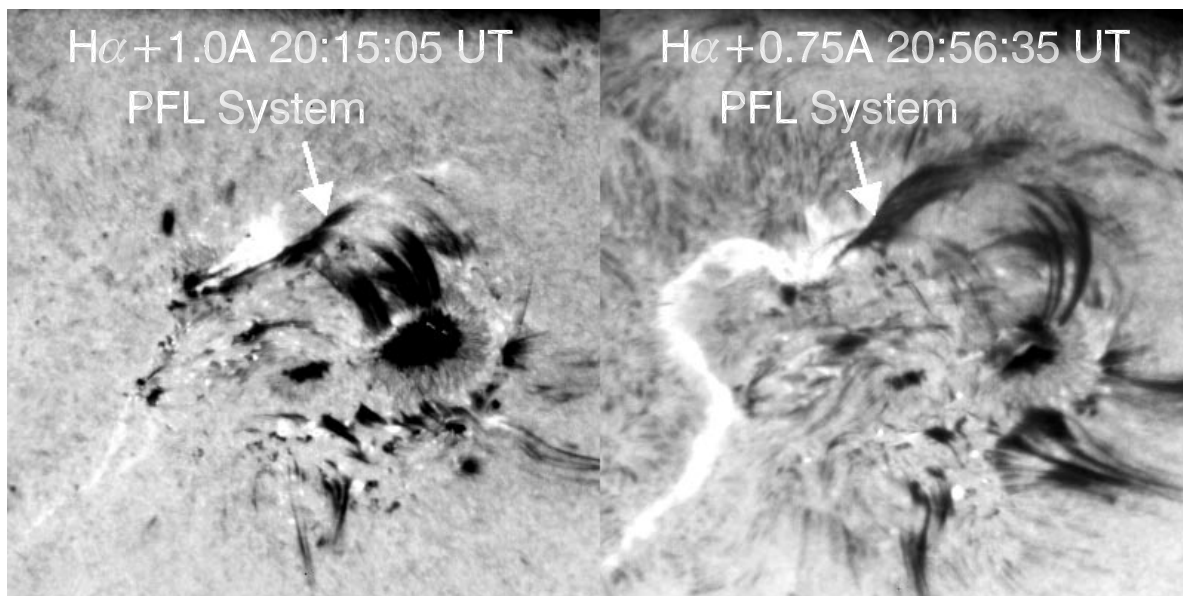


FIG. 3.— $H\alpha$ off-band images of the two-ribbon flare on 1998 November 5. The image at 20:56:35 UT is a contrast-enhanced image. The flare ribbons appear brighter than when it was observed.

release was located at the loop's top in a closed magnetic configuration. They also conjectured that, in the studied flare, a process of driven reconnection between neighboring loops took place.

Gorbachev & Somov (1988) were the first to quantitatively investigate the magnetic topology in an active region. Analyzing the potential field created by four charge points located below the photosphere, they found that the location of observed flare ribbons is in agreement with the simulations. Since then, many studies have shown that chromospheric H α kernels were found to be on the intersection of the separatrices (surfaces that separate volumes of different magnetic connectivity) with the photosphere. But only relatively few studied in detail the magnetic topology in two-ribbon flares (Gorbachev & Somov 1988; Demoulin et al. 1994b; Mandrini et al. 1995; Yurchishin 1997). Both the magnetic configuration and the H α brightenings are found to be qualitatively different and more complex than those proposed in models with open magnetic fields. The studies concluded that the flares under consideration result from the interaction of closed large-scale magnetic structures, and not from an internal instability happening within a twisted flux tube.

Recently, Wang et al. (1999) analyzed the full set of ground- and space-based observational data and came to the conclusion that in many aspects two-ribbon flares are different and they may represent different energy-release events: eruption of sheared loops and interaction of two loops. The major morphological difference is that the former event is associated with opening of the field and the latter is not.

In this paper, we use the Big Bear Solar Observatory (BBSO) high-resolution observation of the longitudinal magnetic field and H α and *Yohkoh* images of Active Region NOAA 8375, as well as a numerical method for reconstruction of the linear force-free field (LFFF), and we show that the 2B/M8.4 two-ribbon flare on 1998 November 5 was a result of many reconnection processes between closed magnetic loops.

2. OBSERVATIONAL DATA AND MAGNETIC FIELD RECONSTRUCTION

BBSO observations completely covered the 1998 November 5 flare, which occurred in AR NOAA 8375. High-resolution H α images were obtained by the 65 cm reflector, with a 0.25 Å bandpass Zeiss filter. The cadence was 30 s with a 0.3 pixel resolution. High-resolution, line-of-sight magnetograms were obtained by the 25 cm refractor. The pixel resolution was 0.5 and the cadence 30 s. The temporal integration of each image was 4 s.

In our analysis, we also used the A11 filter *Yohkoh* soft X-ray data (which cover the lower temperature range). The pixel size of soft X-ray telescope (SXT) images was 5".

Figure 1 shows a *GOES* soft X-ray 1–8 Å flux plot of the 1998 November 5 flare as a function of time. This long-duration event lasted for several hours. The flare started shortly after the very impulsive short-lasting M1.9 flare. No filament was present in this active region prior to onset, so this event is not associated with a filament eruption. Figures 2 and 3 show H α images obtained at the center and at the red wing of the spectral line. As one can see, it was a large flare that extended over the whole active region. The post-flare loop system connected flare ribbons "B" and "C" and showed apparent growth. The off-band images reveal a

strong downflow at the loop footpoints. Further details on this event may be found in Wang et al. (2000).

To reconstruct the coronal three-dimensional magnetic field above the active region, we used a numerical method for the LFFF calculation proposed by Abramenko & Yurchishin (1996). We used the line-of-sight magnetogram of AR 8375 as the photospheric boundary condition. The magnetogram was recorded on 1998 November 5 at 18:18 UT, before the flare onset. The numerical solution was obtained for a three-dimensional volume of size 204" \times 204" \times 204". The size of a grid cell was 2.43 \times 2.43 \times 2.43. We obtained a set of numerical solutions with a different α parameter, and then, for each solution, we calculated the set of field lines. Using high-resolution BBSO H α images, as well as soft X-ray images from *Yohkoh* (Fig. 10 in Wang et al. 2000; Figs. 2 and 6, present paper), we chose the numerical solution ($\alpha = 0.013 \text{ arcsec}^{-1}$) that best fits the observed magnetic configuration before the flare.

3. RESULTS

In our analysis, we used a simple method that allowed us to define magnetic links between the flare ribbons in this two-ribbon flare. First, we calculated the lines of force that originate within the leading spot. The field-line calculations covered the whole sunspot area, and the spatial resolution (i.e., the distance between the two closest footpoints of lines of force) was 2.43 in both directions. Then, considering each line, we located both of its footpoints. Doing so, we could distinguish three different magnetic flux tubes. All the lines of force that originate in the area marked with "a" have their ends at the flare ribbon marked with "B" (Fig. 4, line 1). All the field lines starting from area "b" ended at flare ribbon "A" (Fig. 4, lines 2 and 3), while field lines coming out from area "c" went southeastward and ended at the H α brightening marked "D" (Fig. 5). Any two close magnetic field lines that originated correspondingly in areas "a" and "b," near the border between them, have their second ends separated and rooted in different distant magnetic elements of northern polarity. Thus, the boundaries of these "a,"

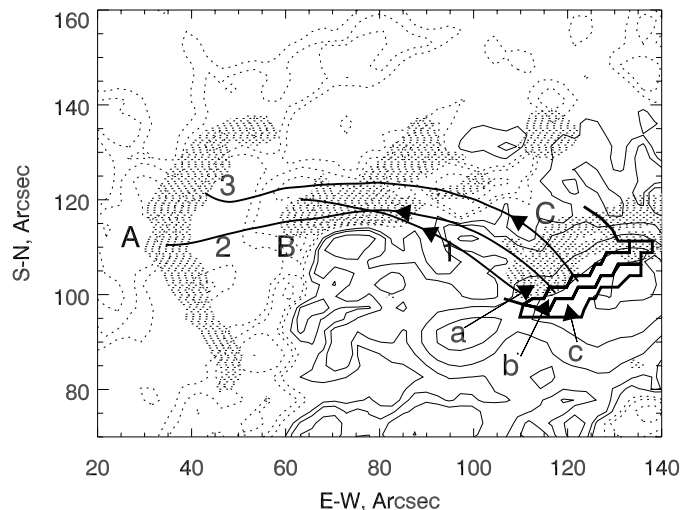


FIG. 4.—AR NOAA 8384, 1998 November 5. Location of H α flare ribbons (dashed area) superposed on a contour map of the longitudinal magnetic field (solid lines: N polarity; dashed lines: S polarity). Contour levels are 100, 200, 400, and 800 G. Solid lines 1, 2, and 3 denote calculated field lines ($\alpha = 0.013 \text{ arcsec}^{-1}$) connecting areas "a" and "b" with the flare ribbons "A" and "B."

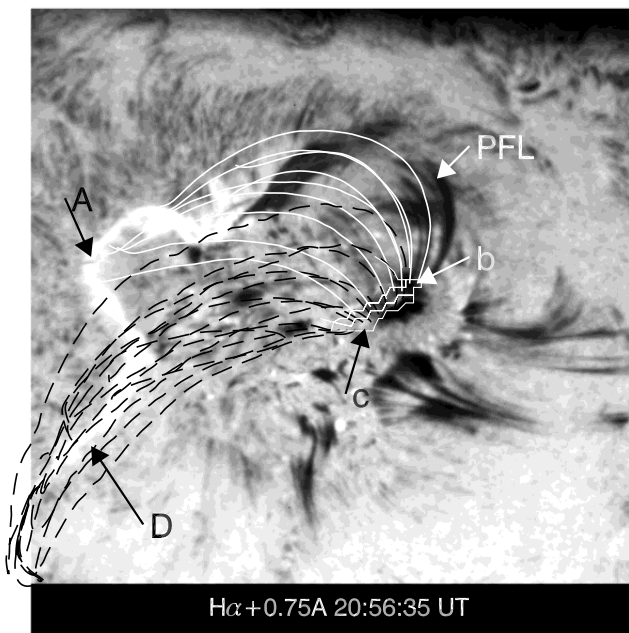


FIG. 5.— $H\alpha + 0.75 \text{ \AA}$ image taken at 20:56:35 UT. Dark loops at upper right: growing postflare loops system. Solid lines denote calculated field lines connecting area “b” with flare ribbon “A.” Dashed lines: calculated field lines ($\alpha = 0.013 \text{ arcsec}^{-1}$), which connect area “c” with the flare ribbon “D.”

“b,” and “c” areas are the intersection of separatrices with the photosphere. In other words, following the definition by Demoulin et al. (1996), these boundaries are places where a drastic change in the field-line linkage occurs. Discontinuities in the field-line linkage at the boundary are at the origin of the formation of current sheets. It has been found that observed flare kernels are located at these discontinuities (Demoulin et al. 1996 and references therein). Our calculations show that, in the case of the 1998 November 5 flare, $H\alpha$ brightenings are also located at places where rapid changes in the field linkage above the photosphere take place. According to this, we are able to clear up the magnetic configuration in the two-ribbon flare as well as indicate magnetic fluxes that took part in the energy-release process.

We suggest that there were at least three large-scale events of energy release. This comes from analysis of the *GOES* light curve (Fig. 1), $H\alpha$ images of the active region (Fig. 2), and the calculated structure of the coronal magnetic field. The first and major energy-release event happened about 19:35 UT (Fig. 1). The $H\alpha$ image taken at 19:43:35 UT (Fig. 2) shows three well-developed flare ribbons, also marked on Figure 4 with letters “A,” “B,” and “C.” We suppose that this energy release was due to the reconnection of two magnetic fluxes, during which the connectivity of the magnetic field was exchanged between four loop footpoints. The first magnetic flux is represented by a line of force marked “1,” which connects area “a” and the flare ribbon “B,” as shown in Figure 4. The second one is a magnetic flux that leaves the leading sunspot in area “b” and goes to flare ribbon “A” (lines 2 and 3). The reconnection will create new magnetic loop systems (see also schematic representation of the magnetic configuration in Fig. 8). The first one, the $H\alpha$ postflare loop system, connects area “b” and flare ribbon “B” (Fig. 4), while the second one, a large-scale

loop system, connects area “a” and flare ribbon “A.” This large-scale loop might correspond to a well-known giant X-ray postflare arch (Švestka et al. 1982). Figure 6 shows the off-band $H\alpha$ image (the same as in Fig. 3) with an overlapped SXT/*Yohkoh* image. One clearly sees the presence of both the low-lying $H\alpha$ postflare loop system (*dark loops*) and the overlying hot X-ray giant coronal arch (*white loop with contours at the top right corner*). The $H\alpha$ loops are located just below the hot X-ray loop, with their tops almost tangential to it. The postflare loop system connects the leading sunspot and the flare ribbon “B,” and the large-scale X-ray arch has its footpoints at the sunspot and the flare ribbon “A.” This kind of magnetic connection corresponds to that predicted by the model. Figure 7 shows the same *Yohkoh* image with the giant postflare arch with overlapped calculated lines of force. The parameter α was equal, in this calculation, to $0.001 \text{ arcsec}^{-1}$. Thus, the observed magnetic configuration entirely supports the inferences obtained from the modeled representation of the magnetic field in the active region.

Both the postflare loop system and the giant X-ray postflare arch exhibit apparent growth (Poletto & Švestka 1992; Schmieder et al. 1995; van Driel-Gesztelyi et al. 1997) as the flare is in progress. Thus, because of the evolution of newly formed loops, a disturbance of the preexisting overlying magnetic field will take place. This, in turn, might provoke the subsequent reconnection of the newly formed loops with the loop system, which connects area “c” and flare ribbon “D” (Fig. 5). If we are correct, this second-step reconnection should start a bit later than the main phase of the energy release. This might be seen in $H\alpha$ images taken at 19:43 UT and 20:18 UT (Fig. 2). One may see that when the eastern ribbon (marked with “A” in Fig. 2) has faded,

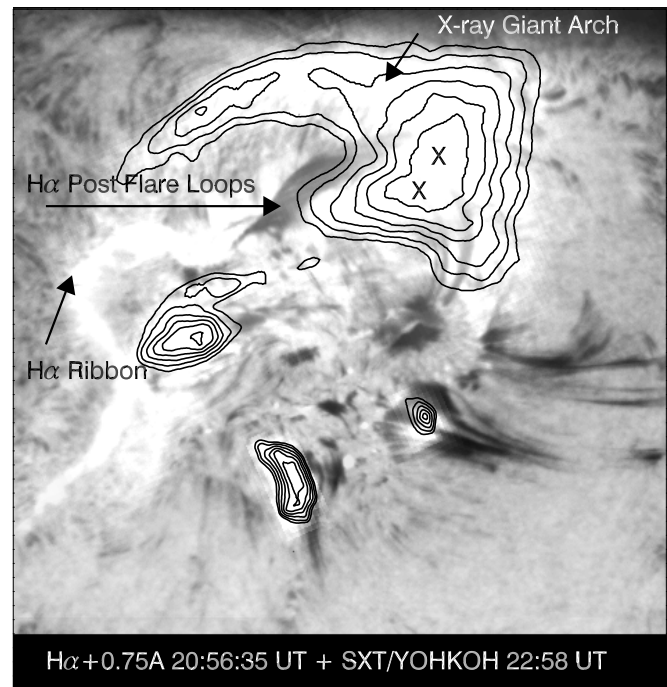


FIG. 6.— $H\alpha + 0.75 \text{ \AA}$ image overlapped by a soft X-ray *Yohkoh* image shows the magnetic configuration after the flare. The resulting configuration consists of the low-lying postflare loops system (*dark loops*) and the overlying giant X-ray postflare arch. The crosses denote the hottest parts of $H\alpha$ and X-ray loops and might locate the site of the reconnection.



FIG. 7.—Soft X-ray *Yohkoh* image and the lines of force of the linear force-free field. Parameter $\alpha = 0.001 \text{ arcsec}^{-1}$.

the southeast ribbon (marked with “D”) becomes brighter. Also, according to Figure 1, at 20:30 UT, after the X-ray flux reached its maximum, the *GOES* light curve has broken its gradual decrease and has formed a plateau, which might imply that an additional source of energy has turned on. This second reconnection event creates a new loop system connecting area “c” with flare ribbon “A” and “b” with “D” (Fig. 5) and explains the evolution of the flare ribbons.

It follows from Figure 8c that there is also a possible third reconnection process that involves magnetic loops aA and bD. After all these steps, the reconnection will be completed, the magnetic field configuration will consist of new disjoint loops (Fig. 8d) and the magnetic field will have a lower amount of energy than it did in the preflare state. The observed evolution of the flare ribbons seems to support the proposed scenario.

A specific feature of this type of reconnection is the exchange of the connectivities of opposite magnetic pol-

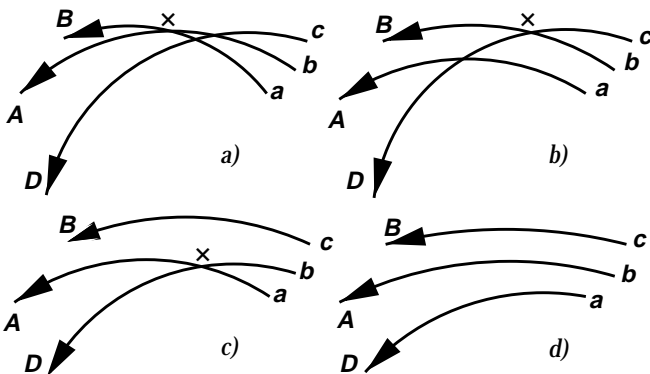


FIG. 8.—Sketch of possible sequence of events that occurred in the 1998 November 5 two-ribbon flare. The cross marks the site of reconnection. The letters denote the loop footpoints and the flare ribbons according to observed picture (see Figs. 3 and 4).

arities without a significant change in the longitudinal field. Analysis of the longitudinal magnetograms supports this theoretical assumption since no large-scale magnetic flux cancellations at, or around, the flare site were observed (Wang et al. 1999).

4. DISCUSSION AND CONCLUSION

The reconnection model of Heyvaerts, Priest, & Rust (1977) suggests a reconnection of oppositely directed fields. Nevertheless, it has been pointed out (Hanaoka 1996) that the observed, interacting flare loops were not necessarily oriented in an antiparallel direction. Moreover, the null points are presented in the magnetic field above the photosphere only when the parasitic bipole is nearly parallel to the large-scale overlying magnetic field (Demoulin, Henoux, & Mandrini 1994a), which can produce a simple loop flare (Heyvaerts et al. 1977). However, configurations without the nulls above the photosphere level could also produce flares (Demoulin et al. 1994a). In the absence of the null point in the magnetic field configuration, Berger (1988), Priest (1988), and then Priest & Forbes (1992) have proposed that the three-dimensional magnetic reconnection may occur at the separatrix layers (Demoulin et al. 1996; Longcope 1996). The typical configuration consists of a pair of two unequally sized loops. The closer footpoints share the same magnetic polarity while the loop planes make some angle in space (Hanaoka 1996, 1997; Nishio et al. 1997; Aschwanden et al. 1999). The magnetic configuration in this interaction can be described in terms of the quadrupolar configuration (Aschwanden et al. 1999). The only possible way of relaxing the preexisting magnetic field is to exchange the connectivities of opposite magnetic polarities. The resulting configuration will consist of two disjoint magnetic loops and will be simplified with reduced differential shear (Schmieder et al. 1996; Abramenko & Yurchishin 1998). This process is in agreement with our present understanding of the evolution of an active region as a continual distortion of an existing equilibrium of the magnetic field with a subsequent fast relaxation to a new neighboring equilibrium (Heyvaerts & Priest 1984; Longcope 1996).

Recently, Aschwanden et al. (1999) studied in great detail quadrupolar magnetic reconnection in solar flares. One finding is that out of 10 studied solar flares six are found with almost collinear interacting loops (the angle between these loops was less than 16°). Another interesting result is based on Melrose’s flare model (Melrose 1997). It has been estimated that only a self-inductance of the largest magnetic loop involved in reconnection is relevant for the free magnetic energy. The amount of the energy depends, to the first order, on the length of the largest loop and the current ratio I_1/I_2 of two interacting loops. The angle between interacting magnetic field lines and their relative distance was found to be of much less importance. The flare energy estimated on the basis of Melrose’s model closely matches the energy inferred from the *GOES* soft X-ray (SXR) flux and hard X-ray telescope (HXT) hard X-ray flux (Aschwanden et al. 1999).

The radiative energy from the SXR-emitting plasma for the 1998 November 5 flare can be estimated by

$$\Delta E^{\text{SXT}} = 3kTn_e fV$$

OR

$$\Delta E^{\text{SXT}} = 3kT \sqrt{fVEM},$$

where T is the plasma temperature, n_e and V are the electron density and the emitting volume correspondingly, f is the filling factor of the SXR loops, $f \leq 1$, and k is the Boltzmann constant. EM is the emission measure of the plasma, which can be expressed as $EM = \int n^2 V$. The plasma parameters can be determined from *GOES* two-channel diagnostics and the loop morphology observed by *SXT* and *TRACE*.

The maximum temperature of the hot plasma was recorded as 20 MK, and the emission measure (EM) of the SXR plasma was $1 \times 10^{50} \text{ cm}^{-3}$. The length and width of the SXR loops can be estimated from *SXT* and *TRACE* images, and the thickness of the loop(s) is taken the same as the loop width; hence the emitting volume V is estimated to be $9 \times 10^{27} \text{ cm}^3$. Taking the filling factor as 1, the electron density of the loops was about $1 \times 10^{11} \text{ cm}^{-3}$. The radiative energy contained in the SXR plasma is, thus, obtained as $4\text{--}7 \times 10^{30}$ ergs if the filling factor is chosen to vary between 0.3 and 1.

To estimate the lower limit of the energy released in the 1998 November 5 flare, we made use of our extrapolated field and Aschwanden et al.'s adoption (Aschwanden et al. 1999) of Melrose's quadrupolar current-loop model. It suggests that the energy released in the flares is due to a redistribution of electric currents and the magnetic flux above the photosphere. The maximum transferable flare energy is defined as

$$\Delta E \approx L_2 \left(\frac{I_2}{I_1} \right)^2 \approx 10^{29.63} \left(\frac{r_2}{10^9 \text{ cm}} \right) \left(\frac{I_2}{10^{11} \text{ A}} \right)^2 \text{ ergs},$$

where r_2 and I_2 are the radius and the current of the large-scale field line involved in the reconnection (Aschwanden et al. 1999). From Figure 4, we estimated the radius r_2 as half the distance between flare ribbon "A" and area "b," and it is equal to $40'' = 3 \times 10^9 \text{ cm}$. Unfortunately, we do not have transverse magnetograms for this active region. To estimate the lower limit of the current I_2 flowing in the large-scale loop, connecting area "b" and flare ribbon "A," we used a linear force-free field transverse magnetogram. Thus, we have obtained the value of the current I_2 equal to $5 \times 10^{10} \text{ A}$. These parameters gave us the value of $\Delta E = 7.5 \times 10^{29}$ ergs, which is 1 order lower than the observational estimates based on the *Yohkoh/SXT* irradiation. The estimation was made assuming the linear force-free magnetic field with $\alpha = \text{constant}$. In this case, the net current I is equal to the total current I_2 of some sign (depends on sign of α) flowing in the coronal loop. However, taking into account the nonlinear character of observed solar magnetic fields and the small-scale structure of the coronal electric currents, it is straightforward to assume that stronger currents are present in coronal loops. Indeed, let us consider a coronal loop that has a nonlinear internal structure with an oscillating α parameter (parameter of the nonlinear force-free field α takes positive and negative

values inside the loop). The net current $I = I_2^+ + I_2^-$ flowing in a coronal loop defines its large-scale structure, in particular, the location of both its footpoints. Then, we can increase or decrease, to some extent, total positive and negative currents I_2^+ and I_2^- , keeping the net current I constant. It would give us unchanged shape of the coronal loop and the constant location of its footpoints, while the internal structure would be more twisted or relaxed. That is the one possible way to increase an amount of currents in a coronal loop. For instance, if we increased the I_2^+ or I_2^- current only by factor of 2, the flare energy ΔE would be equal to 3×10^{30} ergs, which is exactly what we have obtained from the *Yohkoh* observations.

As inferred from LFFF modeling, the two-ribbon flare on 1998 November 5 was a product of a multiple reconnection process between interacting loops, which make a small angle in space. Calculations presented here explore only the large-scale magnetic field structure in the active region. However, taking into account a possible filamentation of the solar magnetic field, this flare could be considered as a superposition of many small-scale reconnection events. In this case, one would expect a variety of angles between small-scale magnetic fluxes, which would bring up the additional energy for the flare (Aschwanden et al. 1999). Another possible scenario is that the self-organized criticality model could be realized with the avalanche process of small-scale energy releases (Lu & Hamilton 1991; Georgoulis & Vlahos 1996).

The magnetic configuration, revealed here, naturally explains the location and the shape of the flare ribbons and the location of the postflare loop system, as well as the magnetic connection between the $H\alpha$ brightenings. Multiple magnetic reconnection also allows us to explain the evolution of the flare ribbons and the additional energy release during the gradual phase of the flare.

The interaction of closed magnetic loops in a two-ribbon flare can also explain the origin of the giant X-ray coronal arch observed after the two-ribbon flare onset (Švestka et al. 1982). This result also meets the conclusion of Šimberova et al. (1993) that the giant arch is the result of progressive reconnection of elementary flux tubes of two (or more) interacting loops.

We would like to emphasize that unlike the Kopp & Pneuman (1976) configuration, the model discussed here does not necessarily need destabilization and eruption of the active region filament. The filament eruption, even if it accompanies a two-ribbon flare, could be one of many equal possibilities to trigger a solar flare.

We acknowledge the referee's comments and suggestions that helped us improve the presentation. This work was supported in part by NSF-ATM (97-14796) and NASA (NAG5-4919) grants.

REFERENCES

- Abramenko, V. I., & Yurchishin, V. B. 1996, *Sol. Phys.*, 168, 47
 ———, 1998, in *ASP Conf. Ser. 155, 2nd Advances in Solar Physics Euro-conference, Three-Dimensional Structure of Solar Active Regions*, ed. C. Alissandrakis & B. Schmieder (San Francisco: ASP), 85
 Aschwanden, M. J., Kosugi, T., Hanaoka, Y., Nishino, M., & Melrose, D. B. 1999, *ApJ*, 526, 1026
 Berger, M. A. 1988, *Proc. Int. Workshop on Reconnection in Space Plasmas Vol. 2* (ESA SP-285; Noordwijk: ESA), 83
 de la Beaujardiere, J.-F., Canfield, R. C., Hudson, H. S., Wulser, J.-P., Acton, L. W., Kosugi, T., & Masuda, S. 1995, *ApJ*, 440, 386
 Demoulin, P., Henoux, J. C., & Mandrini, C. H. 1994a, *A&A*, 285, 1023
 Demoulin, P., Henoux, J. C., Priest, E. R., & Mandrini, C. H. 1996, *A&A*, 308, 643
 Demoulin, P., Mandrini, C. H., Rovira, M. G., Henoux, J.-C., & Machado, M. E. 1994b, *Sol. Phys.*, 150, 221
 Fárnik, F., Švestka, Z., Hudson, H. S., & Uchida, Y. 1996, *Sol. Phys.*, 168, 331
 Forbes, T. G. 1992, in *IAU Colloq. 133, Eruptive Solar Flares*, ed. Z. Švestka, B. V. Jackson, & M. E. Machado (Berlin: Springer), 79
 Georgoulis, M. K., & Vlahos, L. 1996, *ApJ*, 469, L135

- Gorbachev, V. S., & Somov, B. V. 1988, *Sol. Phys.*, 117, 77
Gu, X.-M., Lin, J., Luan, T., & Schmieder, B. 1992, *A&A*, 259, 649
Hanaoka, Y. 1996, *Sol. Phys.*, 165, 275
———. 1997, *Sol. Phys.*, 173, 319
Heinzel, P., Schmieder, B., & Mein, P. 1992, *Sol. Phys.*, 139, 81
Heyvaerts, J., & Priest, E. R. 1984, *A&A*, 137, 63
Heyvaerts, J., Priest, E. R., & Rust D. 1977, *ApJ*, 216, 123
Hirayama, T. 1974, *Sol. Phys.*, 34, 323
Kopp, R. A., & Pneuman, G. W. 1976, *Sol. Phys.*, 50, 85
Kopp, R. A., & Poletto, G. 1990, *Sol. Phys.*, 127, 267
Korobova, Z. B., & Sajdalieva, M. A. 1993, *Sol. Phys.*, 147, 323
Lin, Y.-Z., Zhang, H.-Q., & Zhang, W.-J. 1993, *Sol. Phys.*, 146, 135
Longcope, D. W. 1996, *Sol. Phys.*, 169, 91
Loughhead, R. E., Chen, C.-L., & Wang, J.-L. 1984, *Sol. Phys.*, 92, 53
Lu, E. T., & Hamilton, R. J. 1991, *ApJ*, 380, L89
Mandrini, C. H., Demoulin, P., Rovira, M. G., de La Beaujardière, & Henoux, J.-C. 1995, *A&A*, 303, 927
Melrose, D. B. 1997, *ApJ*, 486, 521
Nishio, M., Yaji, K., Kosugi, T., Nakajima, H., & Sakurai, T. 1997, *ApJ*, 489, 976
Ogir, M. B. 1967, *Bull. Crimean Astrophys. Obs.*, 37, 94
Poletto, G., & Švestka, Z. F. 1992, *Sol. Phys.*, 138, 189
Priest, E. R. 1988, *Proc. Int. Workshop on Reconnection in Space Plasmas Vol. 2 (ESA SP-285; Noordwijk: ESA)*, 73
Priest, E. R., & Forbes, T. G. 1992, *J. Geophys. Res.*, 97(A2), 1521
Roy, J.-R. 1972, *Sol. Phys.*, 26, 418
Rust, D. M., & Bar, V. 1973, *Sol. Phys.*, 33, 459
Schmieder, B. 1992, in *IAU Colloq. 133, Eruptive Solar Flares*, ed. Z. Švestka, B. V. Jackson, & M. E. Machado (Berlin: Springer), 124
Schmieder, B., Demoulin, P., Aulanier, G., & Golub, L. 1996, *ApJ*, 467, 881
Schmieder, B., Heinzel, P., Wiik, J. E., Lemen, J., Anwar, B., Kotrc, P., & Hiei, E. 1995, *Sol. Phys.*, 156, 337
Šimberova, S., Karlicky, M., & Švestka, Z. 1993, *Sol. Phys.*, 146, 343
Smith, S. F., & Ramsey, H. E. 1964, *Z. Astrophys.*, 60, 1
Sturrock, P. A. 1968, in *IAU Symp. 35, Structure and Development of Solar Active Regions*, ed. K. O. Kiepenheuer (New York: Springer), 471
Švestka, Z. 1984, *Sol. Phys.*, 94, 171
Švestka, Z., Fárnik, F., Hudson, H. S., Uchida, Y., Hick, P., & Lemen, J. 1995, *Sol. Phys.*, 161, 331
Švestka, Z., et al. 1982, *Sol. Phys.*, 75, 305
Tang, F. 1985, *Sol. Phys.*, 102, 131
van Driel-Gesztelyi, L., Wiik, J. E., Schmieder, B., Tarbell, T., Kitai, R., Funakoshi, Y., & Anwar, B. 1997, *Solar Phys.*, 174, 151
Vršnak, B., Ruždjak, V., Messerotti, M., & Zlobec, P. 1987, *Sol. Phys.*, 111, 23
Wang, H., et al. 1999, *ApJ*, submitted
Yurchishin, V. B. 1997, *Kinemat. Phys. Celest. Bodies*, 13(6), 33